



Quantum entanglement and criticality in a one-dimensional deconfined quantum critical pointSheng Yang  and Jing-Bo Xu ^{*}*Zhejiang Institute of Modern Physics and Department of Physics, Zhejiang University, Hangzhou 310027, China*

(Received 7 September 2021; accepted 3 December 2021; published 16 December 2021)

We investigate the ground-state quantum entanglement in a one-dimensional incarnation of deconfined quantum critical point by making use of the finite-size density matrix renormalization group method. We observe two distinct behaviors of two-site entanglement calculated on odd and even bonds, and the difference \mathcal{O}_E is shown to obey conventional scaling relations for order parameters. Accurate deconfined critical point and associated critical exponents are numerically extracted from finite-size scaling analyses. We further notice a close similarity between \mathcal{O}_E and the valence-bond-solid order parameter and same observations are also obtained for quantum coherence and trace distance. Furthermore, the deconfined critical point is suggested to possess rich quantum entanglement other than the two-site entanglement from the residual entanglement perspective. Our work explores the critical characteristics of the one-dimensional deconfined quantum critical point from the quantum information aspect and provides insights for its ground-state entanglement structure.

DOI: [10.1103/PhysRevE.104.064121](https://doi.org/10.1103/PhysRevE.104.064121)**I. INTRODUCTION**

Identifying different quantum phases and understanding the quantum phase transitions (QPTs) among them represents one of the most essential tasks in the field of statistical and condensed matter physics [1]. Traditionally, this task can be done within the Landau-Ginzburg-Wilson (LGW) paradigm by recognizing the associated local order parameter and the corresponding symmetry breaking. This approach works well for a large amount of continuous QPTs, while there are also several exceptions that cannot be captured by the LGW description, including topological QPTs [2,3] and deconfined quantum critical points (DQCPs) [4,5]. Therefore, in the past few decades, much research interest has been focused on figuring out the nature of these QPTs and many theoretical as well as numerical tools were developed for this purpose.

The DQCP theory was originally proposed to describe the continuous QPT between an antiferromagnetic phase and a valence-bond-solid (VBS) phase in two-dimensional (2D) quantum Heisenberg magnets [4], which, however, is predicted to be a first-order phase transition according to the LGW theory. As indicated by its name, the DQCP is featured with the deconfined degrees of freedom emerged at the quantum critical point. Although much effort has been put into the numerical simulation of concrete 2D lattice models expected to exhibit DQCP physics [6–21], the nature of the deconfined critical point is still under debate, and the possibility of a weakly first-order QPT with a large correlation length cannot be ruled out due to the observed deviations from finite-size scaling relations [10–13,15]. To investigate more about the essence of the DQCP, it may be necessary to consider physical quantities other than the conventionally studied ones like

magnetization and classical correlation functions. Recently, the frequent communication between quantum information science and condensed matter physics has benefited both areas a lot. Specifically, the concepts from quantum information, such as quantum entanglement [22–24], fidelity [25,26], quantum coherence [27–29], and trace distance [30], have been successfully used to study different QPTs and have provided further perspective on the quantum criticality. Thus it should be worthwhile to explore the behaviors of these quantum information quantities at the deconfined critical points.

On the other hand, several 1D systems [31–36] were also recently shown to share many similarities, like the deconfined degrees of freedom and emergent symmetries occurring at the critical point, with the 2D DQCPs, and the powerful matrix product state (MPS) techniques [37–39] can be fully utilized in these cases. In the present paper, we will focus on the 1D spin chain proposed in Ref. [31], which is predicted to undergo a continuous QPT between a ferromagnetic phase with a broken \mathbb{Z}_2 symmetry and a VBS phase with a broken translation symmetry. By working directly in the thermodynamic limit, two research groups [40,41] independently used the recently developed variational uniform MPS technique [42] combined with the finite entanglement scaling approach [43,44] to study the critical behaviors of the order parameters and classical correlation functions in this 1D DQCP model, from which they extracted accurate values of critical point and critical exponents. It is noted that the simulation results obtained are consistent with the field theory prediction in Ref. [31] and provide strong evidence that the DQCP found in this 1D model is continuous. Later, more investigations were also provided by finite-size scaling analyses of the order parameters and the fidelity susceptibility performed in Refs. [45,46]; the conventional scaling behaviors observed therein make this 1D continuous DQCP even more convincing. However, most of the works mentioned above concentrate mainly on the behaviors of the order parameters and classical

^{*}xujb@zju.edu.cn

correlation functions, and it may be necessary to consider other physical quantities.

Therefore, in this work, we revisited the 1D DQCP put forward in Ref. [31] from a quantum information perspective by performing finite-size density matrix renormalization group (DMRG) calculations in the language of MPS. We computed the quantum entanglement between nearest-neighbor sites and found distinct behaviors for odd and even bonds, from which one can identify the breaking and restoring of the translation symmetry. Based on this observation, a quantity \mathcal{O}_E , the difference of the two-site entanglement on odd and even bonds, was later constructed to study the quantum criticality of the 1D DQCP model by applying a standard finite-size scaling analysis. The numerically obtained quantum critical point and correlation length critical exponent are consistent with previous works. Interestingly, it is shown that this quantity behaves quite like the VBS order parameter in two aspects. First, \mathcal{O}_E decreases from a finite value continuously to zero as the system is tuned from the VBS phase into the ferromagnetic phase. Second, the critical exponent which describes the vanishing pace of \mathcal{O}_E was estimated almost identical with the one for VBS order parameter within numerical accuracy. The same phenomena was also observed when we replaced quantum entanglement with other quantities like quantum coherence and trace distance. Finally, we further explore multipartite entanglement in this 1D DQCP system. The performance of the multipartite entanglement in the thermodynamic limit can be obtained by a simple polynomial fitting based on finite-size systems. It is found that the multipartite entanglement shows a sharp peak at the deconfined critical point, which might be explained by the strong quantum fluctuation and the emerged deconfined degrees of freedom. Our work provides an investigation of the 1D DQCP physics from the quantum information perspective and similar methods may also be applicable to 2D DQCP systems.

This paper is organized as follows. In Sec. II, we describe the model under investigation and briefly review the quantum information concepts used in our work. Then these concepts are applied to study the quantum criticality of the 1D DQCP and the numerical results are presented and analyzed in Secs. III and IV. Finally, we end the paper with a conclusion provided in Sec. V.

II. MODEL AND METHODS

The 1D DQCP model considered here is a linear chain with one spin-1/2 on each site, which was recently proposed in Ref. [31] with the Hamiltonian

$$H = \sum_{i=1}^L (-J_x \sigma_i^x \sigma_{i+1}^x - J_z \sigma_i^z \sigma_{i+1}^z + K_x \sigma_i^x \sigma_{i+2}^x + K_z \sigma_i^z \sigma_{i+2}^z). \quad (1)$$

Here σ_i^α are Pauli operators on the i th site and J_α (K_α) are the nearest-neighbor ferromagnetic (next-nearest-neighbor antiferromagnetic) coupling strengths with $\alpha = x, z$. For simplicity, we fix $K_x = K_z = 1/2$, $J_x = 1$, and leave the coupling J_z to be the only driving parameter. It is shown in Refs. [41,46] that the system exhibits a direct continuous QPT from a translation symmetry-breaking VBS phase into

a \mathbb{Z}_2 symmetry-breaking ferromagnetic phase by varying the driving parameter across the critical point $J_z^c \approx 1.465$. It is also noted that the point $J_z = 1$ (in the VBS phase) represents an exact dimer ground state, called the Majumdar-Ghosh state [47,48],

$$|\text{MG}\rangle = \bigotimes_{m=1}^{L/2} \frac{|\uparrow\rangle_{2m-1} |\uparrow\rangle_{2m} + |\downarrow\rangle_{2m-1} |\downarrow\rangle_{2m}}{\sqrt{2}}, \quad (2)$$

where $|\uparrow\rangle$ and $|\downarrow\rangle$ are the two eigenstates of the Pauli operator σ^z .

As mentioned in Sec. I, this 1D DQCP has been examined from many different aspects [40,41,45,46] and fruitful results have been obtained. However, investigating physical quantities other than the conventionally used order parameters and correlation functions may still be necessary for further research. To this end, we exploit specifically the concepts borrowed from quantum information [49], like quantum entanglement, quantum coherence, and trace distance, to further study the 1D DQCP Hamiltonian (1) in the following.

Since the early 2000s, the connection between quantum information science and QPTs has received much attention and stimulated a large amount of fascinating works. Specifically, this topic begins with the observation of the scaling behaviors of two-site entanglement near quantum critical points [22–24]. Inspired by these pioneering works, different measures of bipartite entanglement were later widely employed in the field of quantum many-body physics to map out the ground-state phase diagrams [50]. Although we have learned a lot from the bipartite entanglement, it is also natural to consider multipartite entanglement, which is believed to reveal a much richer structure of entanglement in many-body states. In this direction, several works [51,52] have shown the possibility of characterizing topological quantum states with multipartite entanglement. In order to understand the entanglement structure of the 1D DQCP more thoroughly, we not only consider bipartite entanglement but also multipartite entanglement in our work. Concretely, we adopt the log-negativity [53] and residual entanglement [54] as the measure of bipartite and multipartite entanglement, respectively. The log-negativity describing the quantum entanglement between two subsystems A and B is computed by

$$E_{\text{ln}}(\rho) = \log_2 \|\rho^{TA}\|_1, \quad (3)$$

where ρ represents the density matrix of the total system, ρ^{TA} is the partial transpose of ρ with respect to subsystem A and $\|\cdot\|_1$ denotes the trace norm. Unlike the log-negativity, the residual entanglement involves N qubits and originates from a monogamy relation of the entanglement of formation [54]. Based on this monogamy relation, the residual entanglement is defined by

$$\tau_i \equiv E_f^2(\rho_{A_i|\bar{A}_i}) - \sum_{j \neq i}^N E_f^2(\rho_{A_i A_j}), \quad (4)$$

where $E_f(\rho_{A_i|\bar{A}_i})$ represents the entanglement of formation [55] between the i th qubit and the rest of the system, and $E_f(\rho_{A_i A_j})$ quantifies the entanglement in the two-qubit system $A_i A_j$. It is noted that the residual entanglement can characterize the quantum entanglement not stored in qubit pairs and

the calculation of $E_f(\rho_{A_i|\bar{A}_i})$ can be simplified to be the von Neumann entropy $S(\rho_{A_i})$ when the many-body state $\rho_{A_1 \dots A_N}$ considered is a pure state [56].

On the other hand, quantum coherence is another important concept in quantum information and its connection with quantum entanglement has been established in some recent works [57,58]. For this reason, it would also be worthwhile to explore quantum coherence in the 1D DQCP model. Specifically, the l_1 norm and relative entropy of coherence are two commonly used measures for quantifying quantum coherence [59]. By fixing a particular reference basis $\{|i\rangle\}_{i=1, \dots, d}$ (in the present work, we specifically choose the direct products of the eigenstates of the Pauli operator σ^z as the reference basis), the l_1 norm of coherence is defined as [59]

$$C_{l_1}(\rho) \equiv \sum_{i \neq j} |\rho_{ij}|, \quad (5)$$

which is simply the sum of the magnitudes of the off-diagonal elements of the density matrix ρ . Staying in the same basis, the relative entropy of coherence, however, involves the concept of von Neumann entropy $S(\rho)$ and is given by [59],

$$C_{\text{re}}(\rho) = S(\rho_{\text{diag}}) - S(\rho), \quad (6)$$

where ρ_{diag} is obtained from ρ by keeping only diagonal entries. In addition to these two measures, there exists other more complicated quantifiers and one can refer to the review in Ref. [60] for more information.

Finally, we also provide some description of the trace distance approach. For two quantum states ρ_1 and ρ_2 in the same Hilbert space, the trace distance is defined by [49]

$$D(\rho_1, \rho_2) \equiv \frac{1}{2} \text{Tr}|\rho_1 - \rho_2|, \quad (7)$$

where $|M| = \sqrt{M^\dagger M}$. It is obvious that the trace distance can be used to quantify the distance between the states ρ_1 and ρ_2 . Therefore, it is intuitive to suggest that the trace distance between a bipartite system ρ_{AB} and the direct product of its two reduced subsystems $\rho_A \otimes \rho_B$ should be able to capture the correlations between the subsystems [61]. Further considering the key role played by correlations in QPTs, one may thus characterize QPTs by employing the trace distance $D(\rho_{AB}, \rho_A \otimes \rho_B)$ [30]. Slightly different from the strategy followed by Ref. [30], where the trace distance method is applied on the whole lattice, we, however, only focus on the central spin pairs in the following to avoid the boundary effect and reduce the computation resource.

So far, we have briefly reviewed the application of quantum information concepts for characterizing quantum phase transitions. It is noted that the methods enumerated above are far from complete and only the concepts relevant to the present work are mentioned. Now we can turn to the investigation of the 1D DQCP physics from a pure quantum information perspective. The DMRG algorithm has been proved to be the most powerful numerical tool for extracting the low-lying physics of 1D lattice systems over the past several decades [37,62,63]. Therefore, to accurately solve the ground state of the Hamiltonian (1) and efficiently obtain the relevant quantities, we perform a finite-size DMRG calculation based on the MPS framework with an open boundary condition. In practice, we consider relatively large system sizes rang-

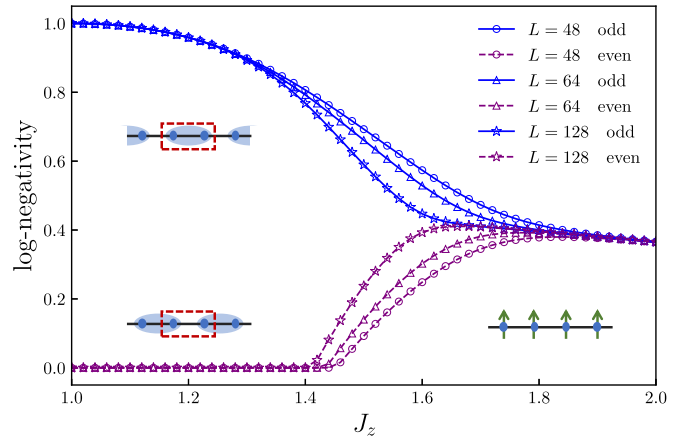


FIG. 1. The log-negativity on the central odd (blue solid line) and even (purple dashed line) bonds as a function of the coupling strength J_z . Different system sizes are denoted by different symbols. The schematic diagrams roughly describe the ground states in the VBS and ferromagnetic phases.

ing from $L = 128$ to 384 with bond dimensions $m = 200$ to 400 to apply reliable finite-size scaling analyses. Specifically, we adopt a sweeping strategy in which the bond dimension is increased from a small value gradually up to the target maximum value in the DMRG processing and the final 30 sweeps are retained for the target bond dimension. The MPS is regarded to have converged to the true ground state of the system once the corresponding energy converges up to the order 10^{-8} . The code of the algorithm is mainly implemented using the ITensor Library [64].

III. SCALING ANALYSES OF QUANTUM INFORMATION QUANTIFIERS FOR 1D DQCP

In this section, we explore the bipartite entanglement in the 1D DQCP model and then study the corresponding critical characteristics by performing a finite-size scaling analysis. Specifically, we calculate the log-negativity of the odd and even bonds in the center of the system to reduce the boundary effect. We first obtain the two-site reduced density matrix of the odd or even bond by tracing out other degrees of freedom in the spin chain from the DMRG ground state and then apply the formula (3) to the reduced density matrix (analogous for other quantities). It is obvious from Fig. 1 that the log-negativity exhibits two distinct behaviors for odd and even bonds as a function of the coupling strength J_z . Since the chain length is chosen to be even, one can expect that the dimers shown in the VBS phase should be built on the odd bonds. In particular, for the Majumdar-Ghosh point ($J_z = 1$), the odd bond is an exact Bell state with maximal entanglement $E_{\text{in}} = 1$, whereas the reduced density matrix of the even bond is $\mathbb{I}_4/4$ with $E_{\text{in}} = 0$. By increasing the coupling J_z from the Majumdar-Ghosh point, the log-negativity of the odd bond gradually decreases while the log-negativity of the even bond remains on the zero value in a large parameter range of the VBS phase and shows a rapid enhancement until the critical point is nearly approached. As the positivity of the log-negativity is a sufficient and necessary condition for the

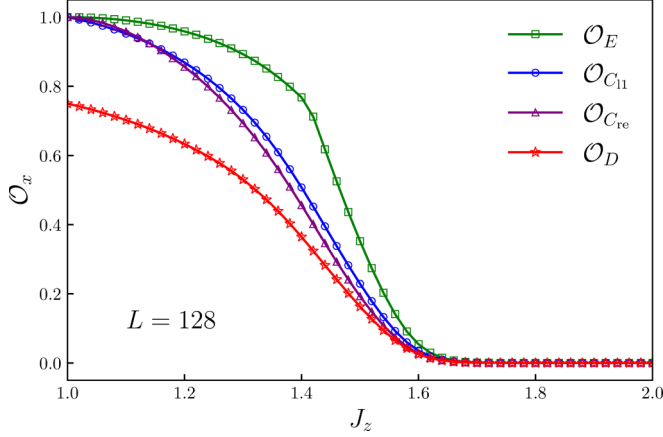


FIG. 2. The breaking and restoring of the translation symmetry can be characterized by the difference of the two-site entanglement on odd and even bonds \mathcal{O}_E . Other quantifiers can also be constructed in a similar way by using quantum coherence ($\mathcal{O}_{C_{1l}}$ and $\mathcal{O}_{C_{re}}$) and trace distance (\mathcal{O}_D).

existence of entanglement in two-qubit mixed states [53,65], the vanishing of the log-negativity indicates a strict absence of quantum entanglement on the even bonds. This suggests that the dimer pattern shown in the VBS phase is rather robust and the dimer picture depicted in Fig. 1 reveals the structure of the underlying two-site entanglement. However, the vanishing of the quantum entanglement of the even bond in the range $J_z \in [1, 1.4]$ is still a nontrivial and interesting result since the ground state is no longer an exact dimer state for $J_z > 1$. We find that the reduced density matrix of the odd and even bonds in the VBS phase can be interpreted as the mixture of the four Bell states, and the behavior of the quantum entanglement in this phase can be explained by the change of the mixing weights of the Bell states, which is detailed in the Appendix.

On the other hand, the log-negativity of the odd and even bonds finally converge in the ferromagnetic phase reflecting the restoring of the translation symmetry. Based on this observation, we introduce the quantity \mathcal{O}_E , which is simply the difference of the two-site entanglement on the odd and even bonds, and its performance as a function of the coupling J_z is displayed in Fig. 2. As one can expect, the quantity \mathcal{O}_E decreases continuously from a finite value to zero as the system is driven from the VBS phase into the ferromagnetic phase, which is reminiscent of the way that order parameters behave in continuous QPTs. This similarity motivates us to consider the following questions: First, how much does this quantity behave like the VBS order parameter? Second, does the quantity \mathcal{O}_E obey finite-size scaling relations? To this end, we need to apply a finite-size scaling analysis to the observable \mathcal{O}_E . Theoretically, an order parameter \mathcal{O}_x characterizing the nature of the associated phase transition follows a universal relation [66]

$$L^{\Delta_x} \mathcal{O}_x = \mathcal{F}_x[L^{1/\nu}(J_z - J_z^c)]. \quad (8)$$

Here Δ_x is the critical exponent describing the vanishing pace of the order parameter, ν is the correlation length critical exponent, \mathcal{F}_x is a homogeneous function, and the subscript “ x ” is

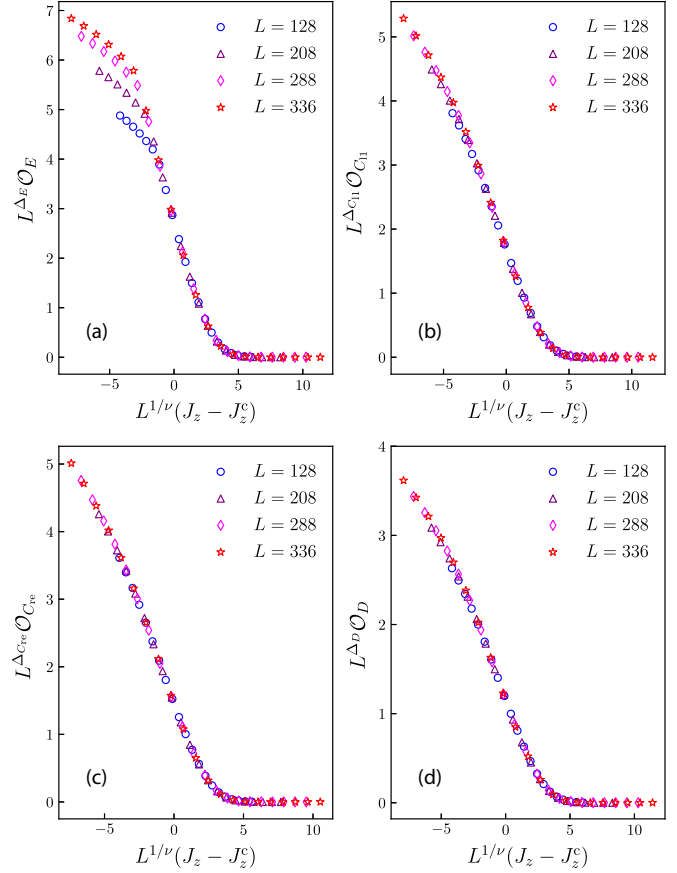


FIG. 3. The confirmation of the universal relation (8) for (a) \mathcal{O}_E , (b) $\mathcal{O}_{C_{1l}}$, (c) $\mathcal{O}_{C_{re}}$, and (d) \mathcal{O}_D within the parameter range $J_z \in (1.3, 1.7)$. By choosing proper values of critical point and exponents, the rescaled quantity $L^{\Delta_x} \mathcal{O}_x$ versus the rescaled driving parameter $L^{1/\nu}(J_z - J_z^c)$ for different system sizes can collapse into a single curve, which is consistent with the finite-size scaling theory. The critical point J_z^c and critical exponents ν and Δ_x obtained in this processing are summarized in Table I.

used to distinguish different quantities. Therefore, we can plot the rescaled entanglement $L^{\Delta_E} \mathcal{O}_E$ as a function of the rescaled coupling $L^{1/\nu}(J_z - J_z^c)$ to confirm the validity of the universal relation (8). By properly choosing the critical point $J_z^c = 1.465$ and critical exponents $\nu = 1.50$ and $\Delta_E = 0.35$ (also see the summary in Table I), we can indeed realize a good collapse of all rescaled curves as shown in Fig. 3(a), which is consistent with the scaling relation (8) for order parameters. Some data in the left part of the plot, however, deviate from the universal relation and our strategy is to make the collapse of the right part as perfect as possible. It is noted that the critical point and the correlation length critical exponent obtained are agreed with the values reported in previous works [41,46]. Thus far, we can answer the questions raised above that the quantity \mathcal{O}_E behaves like an order parameter obeying conventional scaling relations, and furthermore, \mathcal{O}_E has an almost identical critical exponent $\Delta_E = 0.35(1)$ with the VBS order parameter (compared with $\Delta_{\text{VBS}} \equiv \beta/\nu = 0.344(2)$ in the Table I of Ref. [46]). Actually, \mathcal{O}_E can be obtained from the VBS order parameter $\mathcal{O}_{\text{VBS}} \equiv \langle \sigma_1 \cdot \sigma_2 \rangle_{\text{odd}} - \langle \sigma_1 \cdot \sigma_2 \rangle_{\text{even}}$, where σ_1 (σ_2) is the Pauli operator on the first (second) site

TABLE I. The critical point J_z^c and associated critical exponents ν , Δ_x , and $\bar{\Delta}_x$ extracted from the scaling relations (8), (9), and (10) are collected here for comparison. Specifically, the true values obtained from the relations (8) and (10) are estimated by performing full collapses (by adjusting the value of critical point and exponents) of the DMRG data for different system sizes as shown in Figs. 3 and 5, and the uncertainties are determined by detecting the onset of a visible imperfection of the curve collapse. For the $\bar{\Delta}_x$ in Eq. (9), the true value is estimated by performing a linear fitting (based on the least-squares method) using the data for $L = 208, 288, 336$ and the uncertainty is roughly bounded by the fitting using the data for $L = 128, 208, 288, 336$.

Observables	From Eq. (8)			From Eq. (9)	From Eq. (10)			$\nu(\Delta_x + \bar{\Delta}_x)^a$
	J_z^c	ν	Δ_x	$\bar{\Delta}_x$	J_z^c	ν	$\bar{\Delta}_x$	
\mathcal{O}_E	1.465(1)	1.50(4)	0.35(1)	0.340(5)	1.459(1)	1.49(4)	0.338(2)	1.04
$\mathcal{O}_{C_{l1}}$	1.465(1)	1.49(5)	0.34(2)	0.369(10)	1.453(1)	1.50(2)	0.367(1)	1.06
$\mathcal{O}_{C_{re}}$	1.465(2)	1.53(6)	0.34(2)	0.326(5)	1.458(1)	1.52(5)	0.325(2)	1.02
\mathcal{O}_D	1.464(2)	1.50(5)	0.33(2)	0.363(9)	1.453(2)	1.54(3)	0.360(3)	1.04

^aThe ν , Δ_x , and $\bar{\Delta}_x$ involved come from Eqs. (8) and (9).

of the lattice bonds, by replacing the classical correlations with the two-site entanglement. This connection between the quantity \mathcal{O}_E and the VBS order parameter may be used to understand the universal relation followed by the former, while the fact that the critical exponent Δ_E determining the vanishing pace of \mathcal{O}_E is nearly identical with the one for VBS order parameter Δ_{VBS} is still a nontrivial observation and one might treat it as an accident at first sight.

Therefore, our next step is to replace the classical correlations in the VBS order parameter with other quantities, such as quantum coherence and trace distance, to see whether similar phenomena occur in these cases. In Fig. 2, we display the difference of the l_1 norm of coherence $\mathcal{O}_{C_{l1}}$, the relative entropy of coherence $\mathcal{O}_{C_{re}}$, and the trace distance \mathcal{O}_D on the odd and even bonds as a function of the coupling strength J_z . Obviously, all these three quantities can characterize the breaking and restoring of the translation symmetry, respectively, in the VBS and ferromagnetic phases as \mathcal{O}_E does. Moreover, we also confirm the existence of the universal relation for $\mathcal{O}_{C_{l1}}$, $\mathcal{O}_{C_{re}}$, and \mathcal{O}_D independently by performing curve collapses in Figs. 3(b)–3(d) according to the Eq. (8). All the information about the quantum criticality, namely the critical point and associated critical exponents, used in the collapses are collected in the Table I for comparison. There are three points that we would like to note here. First, the curve collapses of quantum coherence and trace distance are better than the one for quantum entanglement, especially for the left part of the function \mathcal{F}_x , which is due to the distinctive behavior of log-negativity on the even bonds. Second, the results of the critical point J_z^c and correlation length critical exponent ν extracted independently from the universal relation of all the four quantum information concepts are consistent with each other, which makes our results more reliable. Third, we also notice that the four critical exponents Δ_E , $\Delta_{C_{l1}}$, $\Delta_{C_{re}}$, and Δ_D are all nearly identical with Δ_{VBS} within numerical accuracy, which seems not to be an accident. This phenomenon may suggest that the nature of the VBS order parameter could still be retained even when the classical correlations in its formula are replaced by other quantifiers. One way to explain this observation may lie in the fact that the main task of VBS order parameter is to characterize the breaking of the translation symmetry, which can be captured by the difference between the odd and even bonds, and thus the use of the classical correlation may not be necessary. To have a more deeper

understanding, however, one may still have to resort to the description of field theories.

Until now, we have explored the quantum criticality of the model by using the universal relation (8) and found a nontrivial similarity between the quantities we used and conventional order parameters. It is noted, however, that this similarity and the universal relation of \mathcal{O}_E may only exist in QPTs having VBS order parameters and the analyses described above may not apply to other QPTs. Nevertheless, the derivative of the two-site quantum entanglement and other quantifiers with respect to the driving parameter seems to be a more useful approach for the study of quantum criticality [22,28,67,68]. Therefore, it would be appealing to investigate the scaling behaviors of $|\partial E_{\text{in}}/\partial J_z|$ calculated on the odd or even bond to study the 1D DQCP model. However, in the following, we still choose to apply the finite-size scaling analysis on quantities $|\partial \mathcal{O}_x/\partial J_z|$ to be an independent examination of the results obtained from Fig. 3. Of course, there should be some connections between the scaling behaviors of $|\partial E_{\text{in}}/\partial J_z|$ and $|\partial \mathcal{O}_E/\partial J_z|$, which will be discussed later.

By numerically calculating the first derivative of the quantities \mathcal{O}_x with respect to the coupling J_z for various system sizes, we can observe sharp peaks of $|\partial \mathcal{O}_x/\partial J_z|$ near the critical point and the peak value $|\partial \mathcal{O}_x/\partial J_z|^m$ is enhanced and the position of the peaks J_z^m moves gradually from the VBS phase toward the critical point as the system size is increased. In the spirit of the finite-size scaling theory, we describe the divergent behavior of $|\partial \mathcal{O}_x/\partial J_z|$ near the critical point by a power law,

$$|\partial \mathcal{O}_x/\partial J_z|^m \sim L^{\bar{\Delta}_x}, \quad (9)$$

where $\bar{\Delta}_x$ is a critical exponent characterizing the diverging pace of $|\partial \mathcal{O}_x/\partial J_z|^m$ with respect to the system size L . Hence, in Fig. 4, we perform linear fittings for $\ln(|\partial \mathcal{O}_x/\partial J_z|^m)$ versus $\ln L$ by the least-squares method. It is obvious that $|\partial \mathcal{O}_x/\partial J_z|^m$ shows a perfect logarithmic divergence with respect to the system size and the critical exponents determined by the slope of fitting lines are collected in Table I for later reference. It is noted that, in the linear fitting processing, we have dropped the data for the smallest $L = 128$ and only make use of the data for the largest three $L = 208, 288, 336$ to obtain more accurate critical exponents $\bar{\Delta}_x$.

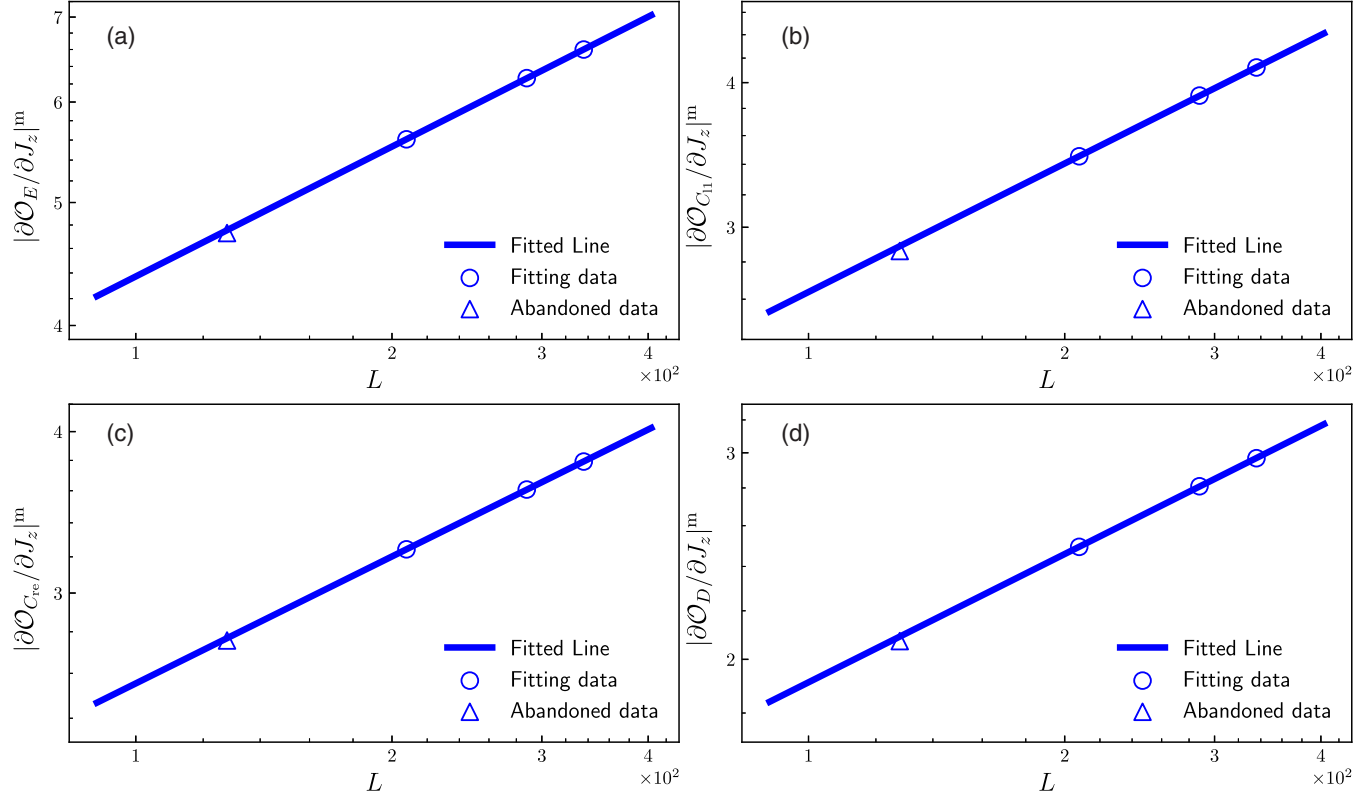


FIG. 4. Logarithmic divergences of the first derivative of (a) \mathcal{O}_E , (b) $\mathcal{O}_{C_{I_1}}$, (c) $\mathcal{O}_{C_{re}}$, and (d) \mathcal{O}_D with respect to the system size. Note that the axes are plotted in a log scale. The solid straight fitted lines are obtained by the least-squares method. The DMRG data used in the fitting processing are marked by open circles while the data abandoned for the smallest $L = 128$ are marked by open triangles. The critical exponents $\bar{\Delta}_x$ obtained are summarized in Table I.

Additionally, the scaling behavior of $|\partial\mathcal{O}_x/\partial J_z|$ near the critical point could also be described by another universal relation

$$L^{-\bar{\Delta}_x}|\partial\mathcal{O}_x/\partial J_z| = \mathcal{G}_x[L^{1/\nu}(J_z - J_z^c)], \quad (10)$$

where \mathcal{G}_x should be the first derivative of the universal function \mathcal{F}_x , and we note the additional minus sign before $\bar{\Delta}_x$ compared with Eq. (8). Therefore, in Fig. 5, we apply the universal relation (10) to all $|\partial\mathcal{O}_x/\partial J_z|$ independently within the coupling range $J_z \in (1.3, 1.7)$. To systematically make a full collapse of the rescaled derivatives $L^{-\bar{\Delta}_x}|\partial\mathcal{O}_x/\partial J_z|$ as a function of the rescaled coupling $L^{1/\nu}(J_z - J_z^c)$ for different system sizes, we first adjust the critical point J_z^c to vertically align the peaks, then vary the exponent $\bar{\Delta}_x$ to have same peak values for all L , and finally fine tune the exponent ν to achieve the curve collapse. All the critical points and critical exponents obtained from the application of Eq. (10) are summarized in Table I. We also note that only the data for $L = 208, 288, 336$ are used in the curve collapses to have a better comparison with the results acquired from Fig. 4.

Now we can focus on the information collected in the Table I to have some discussion about the results obtained so far. First, we can see that the critical exponents extracted independently from Eqs. (8), (9), and (10) are fairly consistent with each other. In order to measure this consistency in a more quantitative way, we further notice an underlying connection

between the critical exponents ν , Δ_x , and $\bar{\Delta}_x$. Since the universal relation (10) could be actually derived from Eq. (8) by taking a first derivative with respect to J_z , the associated critical exponents should obey a simple relation $\nu(\Delta_x + \bar{\Delta}_x) = 1$. It is clear from the last column of the Table I that the relation shown here is satisfied by our numerical results, indicating the finite-size scaling analyses performed are trustworthy. Second, however, we also note that the critical points obtained from Eq. (10) are slightly smaller than the ones acquired from Eq. (8). In fact, a similar situation can be found in the scaling analysis of the fidelity susceptibility performed in the Ref. [45] with a slightly larger obtained critical point. We suspect that this small deviation is caused by the finite-size effect and could be reduced in a controlled way by considering larger system sizes. Finally, we mention that the scaling relations (9) and (10) should also be valid for the first derivatives of the two-site entanglement and other quantifiers calculated on the odd or even bond. Specifically, the critical exponent $\bar{\Delta}_x^{\text{odd}}$ ($\bar{\Delta}_x^{\text{even}}$) for $|\partial E_{\text{in}}/\partial J_z|$ (the log-negativity can be replaced by other quantifiers) on the odd (even) bond could be related with $\bar{\Delta}_x$ through the scaling law (9) by $L^{\bar{\Delta}_x} \sim \alpha L^{\bar{\Delta}_x^{\text{odd}}} + \beta L^{\bar{\Delta}_x^{\text{even}}}$, and we have $\bar{\Delta}_x = \max(\bar{\Delta}_x^{\text{odd}}, \bar{\Delta}_x^{\text{even}})$ in the thermodynamic limit. It is noted that $\bar{\Delta}_x$ (and $\bar{\Delta}_x^{\text{odd/even}}$) differs from the conventional scaling dimension by an additional minus sign, and thus the smaller dimension associated operator is more relevant now becomes the larger one between the odd and even bond is more relevant.

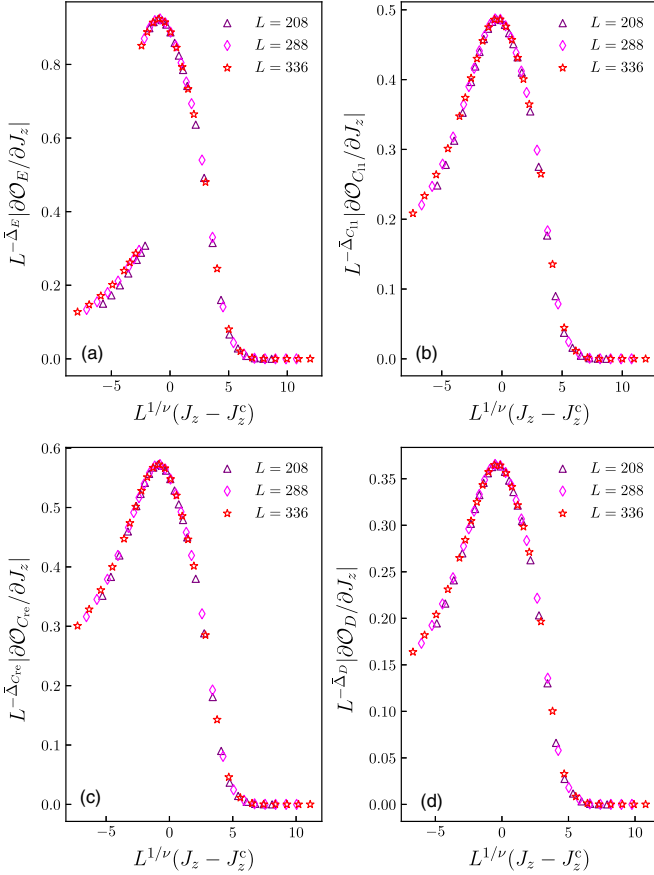


FIG. 5. The application of the universal relation (10) to (a) \mathcal{O}_E , (b) \mathcal{O}_{C_1} , (c) $\mathcal{O}_{C_{re}}$, and (d) \mathcal{O}_D within the parameter domain $J_z \in (1.3, 1.7)$. The critical points J_z^c and associated critical exponents $\bar{\Delta}_x$ and ν used in the collapses are gathered in Table I.

IV. MULTIPARTITE ENTANGLEMENT IN THE 1D DQCP MODEL

In the above, we have investigated the two-site entanglement in the 1D DQCP model and found some interesting results. However, this two-site entanglement is not sufficient to capture the entanglement structure of the ground state and an exploration of the multipartite entanglement seems to be necessary. Therefore, in this section, we further provide an examination about the residual entanglement to have some idea of the entanglement distribution at the deconfined critical point.

Specifically, we apply the residual entanglement on the whole spin chain and, for simplicity, only consider $\tau_{L/2}$ with the partition $A_{L/2}|\bar{A}_{L/2}$, where the definition of A_i can be seen in Eq. (4). It is observed in Fig. 6 that the states deep in the VBS and ferromagnetic phases possess a small residual entanglement as expected, while the states near the critical point show a much richer multipartite entanglement. In addition, we also recognize an obvious L -independent behavior of $\tau_{L/2}$ at both sides of the critical regime. To understand this observation, we need to examine each term of the expression (4). We note that the calculation of the first term $E_f^2(\rho_{A_{L/2}|\bar{A}_{L/2}})$ can be simplified as $S^2(\rho_{A_{L/2}})$, and it is also numerically found that the second term $\sum_{j \neq L/2}^L E_f^2(\rho_{A_{L/2}A_j})$ almost only contains

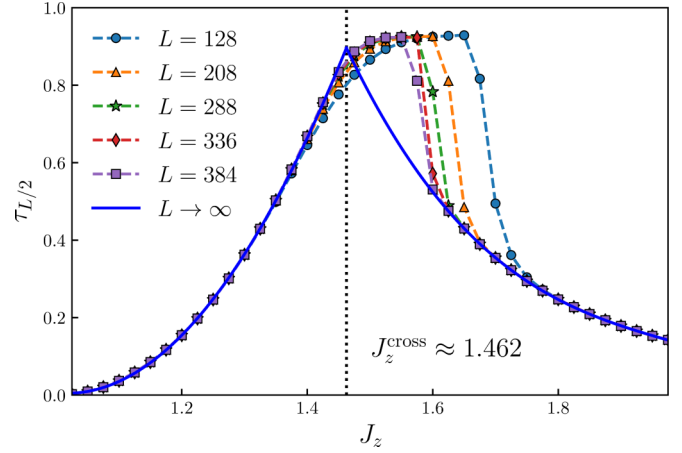


FIG. 6. The residual entanglement $\tau_{L/2}$ as a function of the coupling J_z for different system sizes. To extrapolate to the thermodynamic limit, a second- (third-) degree polynomial function is used to fit the sufficiently converged data in the VBS (ferromagnetic) phase. The quantum critical point J_z^c is roughly estimated by the crossover of the fitted lines.

the contribution from nearest terms. Therefore, the residual entanglement $\tau_{L/2}$ in our case is in some sense a local quantity which depends only on the density matrix of the central spins. Then for a sufficiently large system size L , adding degrees of freedom at the edge of the spin chain should bring negligible influence to the residual entanglement $\tau_{L/2}$ as long as the correlation length is much less than the chain length. This argument could be used to explain not only the L -independent behavior of $\tau_{L/2}$ but also the expanding of the corresponding parameter region toward the critical point as the increase of L . Based on these observations, we can expect to obtain a good approximation of the behavior of $\tau_{L/2}$ in the thermodynamic limit by extrapolating the finite-size results. Specifically, by comparing data for different L , we can determine the parameter region where $\tau_{L/2}$ has sufficiently converged to the infinite L limit. In Fig. 6, these converged data in the VBS and ferromagnetic phases are, respectively, fitted by a second- and third-degree polynomial function and the deconfined critical point is roughly determined as $J_z^c \approx 1.462$ by the crossover of the fitted lines. It is noted that a second-degree polynomial fitting is not good enough for the ferromagnetic region and this is why we adopt a third-degree one there.

Now we can find from Fig. 6 that the deconfined critical point J_z^c displays a large amount of residual entanglement compared with typical VBS and ferromagnetic states, which might be accounted by the strong quantum fluctuation and the gapless deconfined degrees of freedom. Moreover, as mentioned, the residual entanglement can characterize the quantum entanglement not stored in spin pairs, so a large $\tau_{L/2}$ at the critical point indicates the existence of rich entanglement other than the two-site entanglement, like the three-site and four-site entanglement. Hence, it would be appealing to study these various types of entanglement separately in the 1D DQCP model. One way to achieve this is to apply the residual entanglement on the central three or four sites. In this approach, however, the first term in Eq. (4) can no longer be simplified to the von Neumann entropy since the state of

the central three or four spins is in general a mixed state, and the calculation of the residual entanglement would involve an expensive optimization [54]. Due to this restriction, we did not perform such an analysis in the present work. However, we still notice that there exists a related work [67], in which the multipartite entanglement in three or four spins of the 1D XY model is investigated by employing the concept, genuine multipartite negativity. We expect that this multipartite entanglement measure could be used to figure out more details about the structure of quantum entanglement in 1D and 2D DQCP in further studies.

V. CONCLUSION

To summarize, we have investigated the quantum entanglement in the ground state of the 1D DQCP model proposed in Ref. [31] by making use of the large-scale finite-size DMRG algorithm. We have found two distinct behaviors of two-site entanglement on odd and even bonds, and the difference \mathcal{O}_E has been employed to study the critical characteristics. By performing finite-size scaling analyses of \mathcal{O}_E and $|\partial\mathcal{O}_E/\partial J_z|$, we extracted accurate deconfined critical point and associated critical exponents separately from several different aspects. These results were shown to be self-consistent with each other and in agreement with previous works. Meanwhile, we also noticed a similarity between \mathcal{O}_E and the VBS order parameter, and the same observation can be obtained for quantum coherence and trace distance. In addition, the deconfined critical point was argued to possess rich quantum entanglement other than the two-site entanglement from the residual entanglement aspect. Finally, we discussed a possible approach to explore the details of the entanglement structure in this 1D DQCP. Our work provides some insight into the 1D DQCP physics from the quantum information perspective. Recently, a numerical study of the second Rényi entanglement entropy has been performed in a 2D DQCP lattice model [69] and the associated scaling behavior was investigated to understand the underlying DQCP theory. We hope that the methods used in the present work could also be useful for studying 2D DQCPs.

In this work, we have only focused on the ground-state quantum entanglement at the transition. Recently, however, there are also several interesting works [19,70,71] exploring the dynamical aspects of 1D and 2D DQCPs. To expand our current work, an investigation of the quench dynamics of the quantum entanglement in the 1D DQCP spin chain would be a suitable direction for further research.

ACKNOWLEDGMENTS

The authors thank Dr. Guo-Qing Zhang from South China Normal University for helpful discussion and suggestions. This work was supported by the National Natural Science Foundation of China (Grant No. 11975198).

APPENDIX: THE BEHAVIOR OF QUANTUM ENTANGLEMENT IN THE VBS PHASE

In this Appendix, we aim to provide an intuitive explanation to the behavior of the even bond quantum entanglement in the VBS phase observed in Fig. 1. We note that the physical

picture shown here only works for the VBS phase with open boundary condition (nondegenerate ground state) and fails in the ferromagnetic phase (doubly degenerate ground state). The degeneracy of the ground state in each phase can be seen explicitly in Fig. 5(a) of the Ref. [46].

1. Exact form of the reduced density matrix

We first derive an exact form of the two-site reduced density matrix in the VBS phase following the argument given in Ref. [72]. In general, the two-site reduced density matrix can be written as

$$\rho_{ij} = \frac{1}{4} \sum_{\alpha, \beta=0}^3 c_{\alpha\beta}^{ij} (\sigma_i^\alpha \otimes \sigma_j^\beta), \quad (\text{A1})$$

where i and j denote the site position, σ^0 is the identity matrix \mathbb{I}_2 , $\sigma^{1,2,3} = \sigma^{x,y,z}$, and $c_{\alpha\beta}^{ij} = \text{Tr}_{ij}[\rho_{ij}(\sigma_i^\alpha \otimes \sigma_j^\beta)]$. As the reduced density matrix ρ_{ij} is obtained from the ground state of the Hamiltonian, it is natural to expect that the symmetries of the Hamiltonian may give some constraints on the coefficients $c_{\alpha\beta}^{ij}$. For the Hamiltonian studied here [see Eq. (1)], we define three operators $U^\alpha \equiv \bigotimes_{i=1}^L \sigma_i^\alpha$ with $\alpha = x, y, z$. For convenience, we also split these operators into two parts, $U^\alpha = U_{ij}^\alpha \otimes U_{\bar{i}\bar{j}}^\alpha$ with $U_{ij}^\alpha = \sigma_i^\alpha \otimes \sigma_j^\alpha$ and $U_{\bar{i}\bar{j}}^\alpha = \bigotimes_{k \neq i, j} \sigma_k^\alpha$. It is obvious that the Hamiltonian is invariant under the transformation of U^α , namely $U^\alpha H U^\alpha = H$, and it is easy to show that the unique ground state $\rho = |g\rangle\langle g|$ ($|g\rangle$ denote the ground state) has the same property, $U^\alpha \rho U^\alpha = \rho$. By tracing out the degrees of freedom other than the i, j sites (denoted by $\bar{i}\bar{j}$), we can extract the symmetries of the reduced density matrix,

$$\begin{aligned} \rho_{ij} &= \text{Tr}_{\bar{i}\bar{j}}[(U_{ij}^\alpha \otimes U_{\bar{i}\bar{j}}^\alpha) \rho (U_{ij}^\alpha \otimes U_{\bar{i}\bar{j}}^\alpha)] \\ &= \text{Tr}_{\bar{i}\bar{j}}[(U_{ij}^\alpha \otimes U_{\bar{i}\bar{j}}^\alpha U_{\bar{i}\bar{j}}^\alpha) \rho U_{ij}^\alpha] \\ &= \text{Tr}_{\bar{i}\bar{j}}[U_{ij}^\alpha \rho U_{ij}^\alpha] = U_{ij}^\alpha \rho_{ij} U_{ij}^\alpha. \end{aligned} \quad (\text{A2})$$

This constraint greatly simplifies the form of the two-site reduced density matrix. For example, $U_{ij}^z(\sigma_i^x \otimes \sigma_j^0)U_{ij}^z = -\sigma_i^x \otimes \sigma_j^0$ requires a zero c_{10}^{ij} and $U_{ij}^z(\sigma_i^x \otimes \sigma_j^z)U_{ij}^z = -\sigma_i^x \otimes \sigma_j^z$ requires a zero c_{13}^{ij} . After a complete examination of all terms in Eq. (A1), we find there are only four nonzero coefficients $c_{00}^{ij} = 1$, c_{11}^{ij} , c_{22}^{ij} , and c_{33}^{ij} . This means that the two-site reduced density matrix is a Bell diagonal state [73,74], which can be written as the mixture of the four Bell states (from now on, we omit the site indices i and j),

$$\begin{aligned} \rho &= p_1 |\Phi^+\rangle\langle\Phi^+| + p_2 |\Phi^-\rangle\langle\Phi^-| \\ &\quad + p_3 |\Psi^+\rangle\langle\Psi^+| + p_4 |\Psi^-\rangle\langle\Psi^-|, \end{aligned} \quad (\text{A3})$$

where p_k are normalized mixing weights, $|\Phi^\pm\rangle = (|\uparrow\uparrow\rangle \pm |\downarrow\downarrow\rangle)/\sqrt{2}$, and $|\Psi^\pm\rangle = (|\uparrow\downarrow\rangle \pm |\downarrow\uparrow\rangle)/\sqrt{2}$. The quantum entanglement of the Bell diagonal states has been understood quite well [73,75] and the main conclusion is that the necessary and sufficient condition for a Bell diagonal state to be entangled is $\max(p_1, p_2, p_3, p_4) > 1/2$.

2. Perspective from the Bell diagonal state

Now we can use the concept Bell diagonal state to explain the behavior of two-site quantum entanglement in the VBS

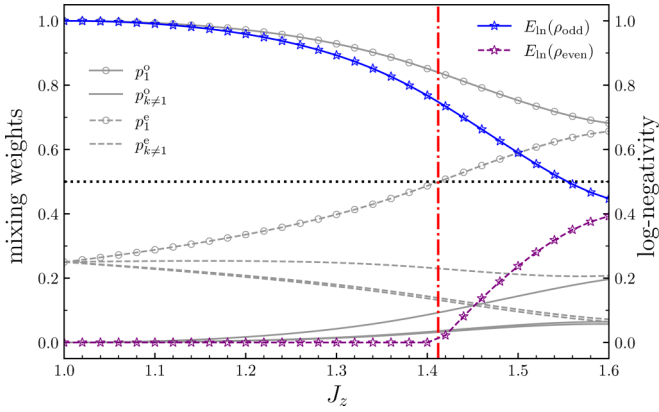


FIG. 7. The mixing weights (left axis) and log-negativity (right axis) of ρ_{odd} and ρ_{even} as a function of the coupling $J_z \in [1., 1.6]$ in the VBS phase with $L = 128$. The red dash-dotted line marks out the point J_z^* , at which the mixing weight p_1^e of the Bell state $|\Phi^+\rangle$ in the density matrix ρ_{even} has increased from $1/4$ up to $1/2$. $E_{\text{ln}}(\rho_{\text{even}})$ becomes finite for $J_z > J_z^*$.

phase shown in Fig. 1. According to the above discussion, the reduced density matrix ρ_{odd} (ρ_{even}) of the odd (even) bond should be a Bell diagonal state which has also been confirmed by the DMRG numerical results for $J_z \in [1, 1.62]$ with $L = 128$. For $J_z > 1.62$, the ground state becomes doubly degenerate and the associated reduced density matrix is no longer a Bell diagonal state and we do not discuss this parameter range in the following. However, we still numerically find that ρ_{odd} and ρ_{even} have a simple structure for $J_z > 1.62$ and the inversion symmetry [31] may help to determine the exact form.

To analyze the quantum entanglement of the odd and even bonds in the VBS phase, we start with the exact Majumdar-Ghosh point $J_z = 1$. At this point, the density matrix ρ_{odd}

only has the contribution from the component $|\Phi^+\rangle$ ($p_1^o = 1$), while ρ_{even} is a mixture of all Bell states with equal weights ($p_k^e = 1/4$). By increasing the coupling J_z , the translation symmetry will be restored gradually. In the Bell diagonal state picture, we can expect that the change of the mixing weights p_k^o and p_k^e should reflect this symmetry restoring. Therefore, we plot the mixing weights of ρ_{odd} and ρ_{even} as a function of the coupling J_z within the VBS phase. It is obvious from Fig. 7 that the distribution of the mixing weights p_k^o and the distribution of p_k^e become more and more closed to each other with the increasing of J_z , which implies the restoring of the translation symmetry. Moreover, it is noted that all mixing weights p_k^e of the reduced density matrix ρ_{even} remain smaller than $1/2$ in the range $J_z \in [1, 1.4]$. This means that there is no quantum entanglement between the two spins on the even bond, which is consistent with the vanishing of the log-negativity $E_{\text{ln}}(\rho_{\text{even}})$ shown in Figs. 1 and 7. These two spins are entangled only when the mixing weight p_1^e becomes larger than $1/2$ ($J_z \gtrsim 1.41$). This completes our discussion of the two-site quantum entanglement in the VBS phase.

To summarize, we have provided an intuitive explanation to the absence of the quantum entanglement on the even bond shown in Fig. 1. The Bell diagonal state picture used here may not work for general quantum spin models; however, it shows the possibility of employing the quantum information concepts to investigate the physics of quantum many-body systems, like the restoring of broken symmetry and the closing of the energy gap. On the other hand, we also show a potential connection between the symmetries of the Hamiltonian and the reduced density matrix obtained from a nondegenerate ground state. However, many interesting quantum phases are generally gapless, therefore, finding a systematic way to extract the symmetry of the reduced density matrix from the Hamiltonian symmetry for gapless phases would be an interesting problem to be solved.

- [1] S. Sachdev, *Quantum Phase Transitions*, 2nd ed. (Cambridge University Press, Cambridge, UK, 2011).
- [2] J. M. Kosterlitz and D. J. Thouless, *J. Phys. C* **6**, 1181 (1973).
- [3] F. D. M. Haldane, *Phys. Rev. Lett.* **50**, 1153 (1983).
- [4] T. Senthil, A. Vishwanath, L. Balents, S. Sachdev, and M. P. A. Fisher, *Science* **303**, 1490 (2004).
- [5] T. Senthil, L. Balents, S. Sachdev, A. Vishwanath, and M. P. A. Fisher, *Phys. Rev. B* **70**, 144407 (2004).
- [6] A. W. Sandvik, *Phys. Rev. Lett.* **98**, 227202 (2007).
- [7] R. G. Melko and R. K. Kaul, *Phys. Rev. Lett.* **100**, 017203 (2008).
- [8] A. B. Kuklov, M. Matsumoto, N. V. Prokof'ev, B. V. Svistunov, and M. Troyer, *Phys. Rev. Lett.* **101**, 050405 (2008).
- [9] J. Lou, A. W. Sandvik, and N. Kawashima, *Phys. Rev. B* **80**, 180414(R) (2009).
- [10] A. W. Sandvik, *Phys. Rev. Lett.* **104**, 177201 (2010).
- [11] A. Banerjee, K. Damle, and F. Alet, *Phys. Rev. B* **82**, 155139 (2010).
- [12] K. Harada, T. Suzuki, T. Okubo, H. Matsuo, J. Lou, H. Watanabe, S. Todo, and N. Kawashima, *Phys. Rev. B* **88**, 220408(R) (2013).
- [13] K. Chen, Y. Huang, Y. Deng, A. B. Kuklov, N. V. Prokof'ev, and B. V. Svistunov, *Phys. Rev. Lett.* **110**, 185701 (2013).
- [14] S. Pujari, K. Damle, and F. Alet, *Phys. Rev. Lett.* **111**, 087203 (2013).
- [15] H. Shao, W. Guo, and A. W. Sandvik, *Science* **352**, 213 (2016).
- [16] T. Sato, M. Hohenadler, and F. F. Assaad, *Phys. Rev. Lett.* **119**, 197203 (2017).
- [17] H. Shao, Y. Q. Qin, S. Capponi, S. Chesi, Z. Y. Meng, and A. W. Sandvik, *Phys. Rev. X* **7**, 041072 (2017).
- [18] X.-F. Zhang, Y.-C. He, S. Eggert, R. Moessner, and F. Pollmann, *Phys. Rev. Lett.* **120**, 115702 (2018).
- [19] N. Ma, G.-Y. Sun, Y.-Z. You, C. Xu, A. Vishwanath, A. W. Sandvik, and Z. Y. Meng, *Phys. Rev. B* **98**, 174421 (2018).
- [20] J. Wildeboer, N. Desai, J. D'Emidio, and R. K. Kaul, *Phys. Rev. B* **101**, 045111 (2020).
- [21] B. Zhao, J. Takahashi, and A. W. Sandvik, *Phys. Rev. Lett.* **125**, 257204 (2020).

- [22] A. Osterloh, L. Amico, G. Falci, and R. Fazio, *Nature (London)* **416**, 608 (2002).
- [23] T. J. Osborne and M. A. Nielsen, *Phys. Rev. A* **66**, 032110 (2002).
- [24] G. Vidal, J. I. Latorre, E. Rico, and A. Kitaev, *Phys. Rev. Lett.* **90**, 227902 (2003).
- [25] H. T. Quan, Z. Song, X. F. Liu, P. Zanardi, and C. P. Sun, *Phys. Rev. Lett.* **96**, 140604 (2006).
- [26] P. Zanardi and N. Paunković, *Phys. Rev. E* **74**, 031123 (2006).
- [27] G. Karpat, B. Çakmak, and F. F. Fanchini, *Phys. Rev. B* **90**, 104431 (2014).
- [28] Y.-C. Li and H.-Q. Lin, *Sci. Rep.* **6**, 26365 (2016).
- [29] J.-J. Chen, J. Cui, Y.-R. Zhang, and H. Fan, *Phys. Rev. A* **94**, 022112 (2016).
- [30] D.-W. Luo and J.-B. Xu, *Ann. Phys.* **354**, 298 (2015).
- [31] S. Jiang and O. Motrunich, *Phys. Rev. B* **99**, 075103 (2019).
- [32] C. Mudry, A. Furusaki, T. Morimoto, and T. Hikihara, *Phys. Rev. B* **99**, 205153 (2019).
- [33] M. Weber, F. Parisen Toldin, and M. Hohenadler, *Phys. Rev. Research* **2**, 023013 (2020).
- [34] S. Yang, D.-X. Yao, and A. W. Sandvik, Deconfined quantum criticality in spin-1/2 chains with long-range interactions, [arXiv:2001.02821](https://arxiv.org/abs/2001.02821) (2020).
- [35] B. Roberts, S. Jiang, and O. I. Motrunich, *Phys. Rev. B* **103**, 155143 (2021).
- [36] T. Ogino, R. Kaneko, S. Morita, S. Furukawa, and N. Kawashima, *Phys. Rev. B* **103**, 085117 (2021).
- [37] U. Schollwöck, *Ann. Phys.* **326**, 96 (2011).
- [38] R. Orús, *Ann. Phys.* **349**, 117 (2014).
- [39] S. Paeckel, T. Köhler, A. Swoboda, S. R. Manmana, U. Schollwöck, and C. Hubig, *Ann. Phys.* **411**, 167998 (2019).
- [40] B. Roberts, S. Jiang, and O. I. Motrunich, *Phys. Rev. B* **99**, 165143 (2019).
- [41] R.-Z. Huang, D.-C. Lu, Y.-Z. You, Z. Y. Meng, and T. Xiang, *Phys. Rev. B* **100**, 125137 (2019).
- [42] V. Zauner-Stauber, L. Vanderstraeten, M. T. Fishman, F. Verstraete, and J. Haegeman, *Phys. Rev. B* **97**, 045145 (2018).
- [43] L. Tagliacozzo, T. R. de Oliveira, S. Iblisdir, and J. I. Latorre, *Phys. Rev. B* **78**, 024410 (2008).
- [44] F. Pollmann, S. Mukerjee, A. M. Turner, and J. E. Moore, *Phys. Rev. Lett.* **102**, 255701 (2009).
- [45] G. Sun, B.-B. Wei, and S.-P. Kou, *Phys. Rev. B* **100**, 064427 (2019).
- [46] Q. Luo, J. Zhao, and X. Wang, *Phys. Rev. B* **100**, 121111(R) (2019).
- [47] C. K. Majumdar and D. K. Ghosh, *J. Math. Phys.* **10**, 1388 (1969).
- [48] C. K. Majumdar and D. K. Ghosh, *J. Math. Phys.* **10**, 1399 (1969).
- [49] M. A. Nielsen and I. L. Chuang, *Quantum Computation and Quantum Information: 10th Anniversary Edition* (Cambridge University Press, Cambridge, UK, 2010).
- [50] L. Amico, R. Fazio, A. Osterloh, and V. Vedral, *Rev. Mod. Phys.* **80**, 517 (2008).
- [51] L. Pezzè, M. Gabbriellini, L. Lepori, and A. Smerzi, *Phys. Rev. Lett.* **119**, 250401 (2017).
- [52] Y.-R. Zhang, Y. Zeng, H. Fan, J. Q. You, and F. Nori, *Phys. Rev. Lett.* **120**, 250501 (2018).
- [53] G. Vidal and R. F. Werner, *Phys. Rev. A* **65**, 032314 (2002).
- [54] Y.-K. Bai, Y.-F. Xu, and Z. D. Wang, *Phys. Rev. Lett.* **113**, 100503 (2014).
- [55] W. K. Wootters, *Phys. Rev. Lett.* **80**, 2245 (1998).
- [56] G.-Q. Zhang, W. Wu, and J.-B. Xu, *Phys. Rev. A* **96**, 032302 (2017).
- [57] A. Streltsov, U. Singh, H. S. Dhar, M. N. Bera, and G. Adesso, *Phys. Rev. Lett.* **115**, 020403 (2015).
- [58] E. Chitambar and M.-H. Hsieh, *Phys. Rev. Lett.* **117**, 020402 (2016).
- [59] T. Baumgratz, M. Cramer, and M. B. Plenio, *Phys. Rev. Lett.* **113**, 140401 (2014).
- [60] A. Streltsov, G. Adesso, and M. B. Plenio, *Rev. Mod. Phys.* **89**, 041003 (2017).
- [61] A. Smirne, H.-P. Breuer, J. Piilo, and B. Vacchini, *Phys. Rev. A* **82**, 062114 (2010).
- [62] S. R. White, *Phys. Rev. Lett.* **69**, 2863 (1992).
- [63] S. R. White, *Phys. Rev. B* **48**, 10345 (1993).
- [64] M. Fishman, S. R. White, and E. M. Stoudenmire, The ITensor software library for tensor network calculations, [arXiv:2007.14822](https://arxiv.org/abs/2007.14822) (2020).
- [65] M. Horodecki, P. Horodecki, and R. Horodecki, *Phys. Lett. A* **223**, 1 (1996).
- [66] G. Nigel, *Lectures on Phase Transitions and the Renormalization Group*, 1st ed. (CRC Press, Boca Raton, FL, 1992).
- [67] M. Hofmann, A. Osterloh, and O. Gühne, *Phys. Rev. B* **89**, 134101 (2014).
- [68] J.-Q. Cheng and J.-B. Xu, *Phys. Rev. E* **97**, 062134 (2018).
- [69] J. Zhao, Y.-C. Wang, M. Cheng, and Z. Y. Meng, Scaling of entanglement entropy at deconfined quantum criticality, [arXiv:2107.06305](https://arxiv.org/abs/2107.06305) (2021).
- [70] G. Sun and B.-B. Wei, *Phys. Rev. B* **102**, 094302 (2020).
- [71] R.-Z. Huang and S. Yin, *Phys. Rev. Research* **2**, 023175 (2020).
- [72] Q. Chen, G.-Q. Zhang, J.-Q. Cheng, and J.-B. Xu, *Quant. Inf. Process.* **18**, 8 (2018).
- [73] R. Horodecki and M. Horodecki, *Phys. Rev. A* **54**, 1838 (1996).
- [74] M. D. Lang and C. M. Caves, *Phys. Rev. Lett.* **105**, 150501 (2010).
- [75] R. Horodecki, P. Horodecki, M. Horodecki, and K. Horodecki, *Rev. Mod. Phys.* **81**, 865 (2009).